Proceedings of the ASME Conference on Smart Materials, Adaptive Structures and Intelligent Systems
SMASIS2008
October 28-30, 2008, Ellicott City, Maryland, USA

SMASIS2008- 482

IMPROVED PREDICTION OF ELECTRODES' MASS LOADING EFFECT ON MEMS FBAR STRUCTURE IN LONGITUDINAL RESONANCE

Annie Ruimi
Department of Mechanical Engineering
Texas A&M University at Qatar
Qatar

Yueming Liang
Exxon Mobile
Houston,Texas

Robert M. McMeeking
Department of Mechanical Engineering,
Materials Department,
University of California, Santa Barbara,
California

ABSTRACT

In this paper, we derive an exact one-dimensional rule for predicting mass loading effect due to electrodes by analyzing a FBAR structure consisting of a piezoelectric layer and two electrodes in longitudinal resonance. We validate the numerical scheme using aluminum nitride as the piezoelectric material and gold and aluminum for the top and bottom electrodes respectively. Results are compared with three-dimensional finite elements simulations obtained earlier. It is seen that the new rule predicts higher values of the resonant frequency and constitutes an improvement over an elementary rule particularly for electrodes thicknesses greater than 20% of the piezoelectric layer thickness.

INTRODUCTION

Arrays of microelectromechanical (MEM) film bulk acoustic resonators (FBARs) are widely used in the communication industry as RF filters in the ultra-high-frequency regime [1]-[9]. A one-dimensional analysis shows that for an ideal FBAR resonator consisting of a piezoelectric layer alone, i.e. a device with electrodes of negligible thickness, the first longitudinal resonance is inversely proportional to the layer's thickness [10]-[12] according to the relation f=V/2h where V is the material's acoustic velocity and h the piezoelectric plate thickness, allowing structures a few microns thick to have the potential of reaching the frequencies in the GHz range such are those needed for wireless communication devices [1]. However there is practical limit to how thin electrodes might be and inevitably, the effect of electrode thickness must be taken into account in the analysis to accurately predict the performance of FBAR resonators. FBAR device performance is mainly evaluated by means of the effective acoustic coupling coefficient K^2 and the quality factor Q [11]-[12]. K^2 combines the elastic, piezoelectric and dielectric material coefficients and is a measure of the ability of the piezoelectric material to convert electrical energy into mechanical energy. High values of K^2 are desirable and indicate low insertion loss. The quality factor Q measures mechanical losses due to damping and is an indication of the sharpness of the resonant response of the system [10]-[12]. Values of Q on the order of 10^3 are expected in electronic applications such as those discussed but imply very low damping coefficients which has been proven difficult to achieve in practice because of the complex geometry of FBAR devices and the many locations where energy can dissipate [1]-[9]. Multiple collaborative efforts to study FBAR loss mechanisms and to improve their performance have taken place during the last ten years [1]-[9], [14]-[16]. Recently, three teams (Fabrication, Materials Processing and Simulations) at the University of California at Santa Barbara (UCSB) have taken part in this research effort. Measurements of a beam-supported aluminum nitride FBAR device also fabricated in the UCSB facility were compared with three-dimensional results. The simulations were performed with the commercial software Abaqus. The simulation team has

focused on provide information useful to researchers at the design stages since fabricating in the lab various configurations of resonators would be extremely difficult and costly. The device fabricated at UCSB and the mesh used in the simulations are shown on Figure 1. We also compared three-dimensional finite element results to one-dimensional analytical ones with the goal of determining if a three-dimensional analysis was necessary to evaluate the performance of the device or if certain key parameters could be evaluated with a simple one-dimensional analysis. This is the object of this paper.

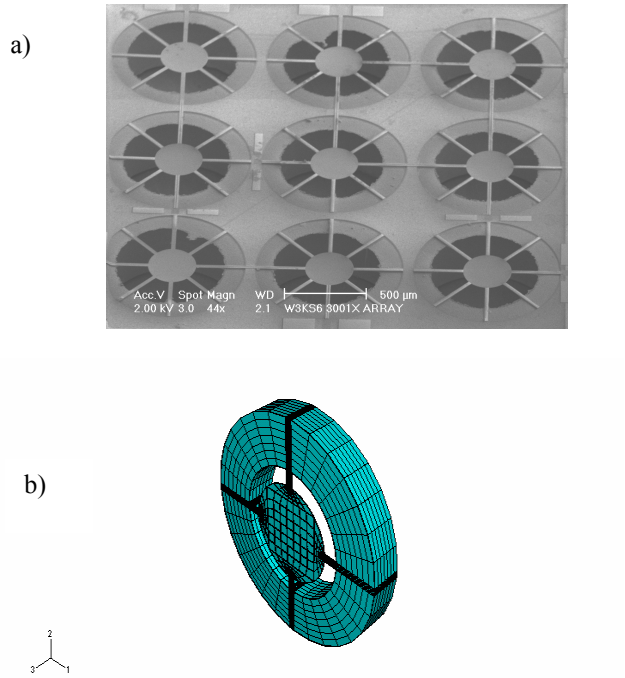

Figure 1. a) 3x3 Array of AlN trampoline resonators fabricated at UCSB (reproduced with permission of N. C. Mac Donald et al. at UCSB) and b) the Finite Element mesh of the trampoline resonator used in simulations.

The immediate effect of taking into account the effect of electrodes in FBAR studies is the decrease of the value of the resonant frequency of the resonating system according to a one-dimensional spring-mass system model [10]-[13] and known as mass loading effect. This in turn, affects the K^2 and Q parameters as they are directly related to the pair of resonant frequencies which occur in piezoelectric materials: the frequency that will cause the electric impedance to be zero is the resonant frequency f_R and the one which will result in an infinite electric impedance is called the anti-resonant frequency f_a [10], so strictly speaking, the frequency which is inversely proportional to the piezoelectric layer's thickness discussed above is the anti-resonant frequency.

To evaluate the (anti)-resonant frequency of a structure consisting of more than one piezoelectric film, a simple rule used in practice [11] is to approximate its value as $f=1/2\,(h_1/2V_1+ h_2/2V_2+h_3/2V_3)^{-1}$ where the h's refer to the thickness of each material layer and the V's are the associated acoustic velocities. Note that for electrodes of negligible thickness, we recover $f=V_1/2h_1$ as described above. In this paper, we derive a one-dimensional rule for mass loading effect due to electrodes by analyzing a composite FBAR structure consisting of a piezoelectric layer sandwiched between two electrodes. The device is placed in an electrical field directed along the device thickness. The electrode's faces are orthogonal to the axis of polarization so that through-thickness vibrations result. We validate the analytical scheme using aluminum nitride (AlN) as the piezoelectric material and gold and aluminum as the top and bottom electrodes respectively. Results are compared against three-dimensional finite element simulations values we obtained earlier. Details of the device fabricated at UCSB and the material processing techniques used can be found in [16]-[18] while the methodology used in the finite element simulations of the resonator can be found in [19]-[20].

DEVICE DESCRIPTION

The geometry of the device simulated is depicted on Figure 2 a. It consists of a trampoline shape resonator, i.e. a circular resonator 300 μm in diameter suspended over an air cavity supported by four beams 300 μm long and 24 μm wide. Both the circular resonator and the beams are made of AlN. The piezoelectric layer is sandwiched between a gold and an aluminum electrode. The gold electrode covers the circular portion of the resonator only. Aluminum nitride was chosen for its desirable properties: a high acoustic velocity (~11000m/s), a good effective coupling coefficient (K^2~6.2%) and piezoelectric coefficient (1.55 C/m2) and a coefficient of thermal expansion comparable to that of silicon [14]. AlN is also process compatible with silicon technology [14]. With such acoustic velocity, an ideal FBAR device made of an aluminum nitride layer 1.7 μm thick and electrodes of negligible thickness, would resonate at 3.2 GHz. The device is forced by an electric filed oriented perpendicular to the electrodes faces. The mechanical and boundary conditions enforced in the simulations are shown on Figure 2 b. The aluminum nitride top surface is maintained at a constant potential while the bottom surface is fixed at zero potential. Thin layers of nickel and aluminum respectively 0.04 μm and 0.02 μm each were initially added at the fabrication stages but were later abandoned in view of the difficulties associated. A set of simulations take them into account (5-layer simulations) while another set does not (3-layer simulations). In both models, the support-beams are prevented any displacement which limits the dissipation of energy between the resonator and its immediate surrounding. Material damping as a form known as Raleigh damping is accounted for in the simulations.

THEORY

We recall that the three-dimensional constitutive equations of lossless piezoelectric materials, assuming constant temperature, are given in a body of volume V by

$$\begin{aligned} \{\mathbf{T}\} &= [\mathbf{c}^{\mathbf{E}}]\{\mathbf{S}\} - [\mathbf{e}]^{\mathbf{T}}\{\mathbf{E}\} \\ \{\mathbf{D}\} &= [\mathbf{e}]\{\mathbf{S}\} + [\boldsymbol{\varepsilon}^{\mathbf{S}}]\{\mathbf{E}\}, \end{aligned} \tag{1}$$

where in Cartesian coordinates, $\{\mathbf{T}\}^{\mathbf{T}} = \{T_{11}\ T_{22}\ T_{33}\ T_{23}\ T_{13}\ T_{12}\}$ is the array of stress components, the superscript *T* indicating the transpose, $\{\mathbf{S}\}^{\mathbf{T}} = \{S_{11}\ S_{22}\ S_{33}\ S_{23}\ S_{13}\ S_{12}\}$ is the array of strain components, $\{\mathbf{E}\}^{\mathbf{T}} = \{E_1\ E_2\ E_3\}^T$ is the array of electric field components, and $\{\mathbf{D}\}^{\mathbf{T}} = \{D_1\ D_2\ D_3\}^T$ is the array of

components of electric displacements [10]. In the context of small deformation theory, the components of strain are given in terms of the displacement components u_i, as $S_{ij}=(u_{i,j} + u_{j,i})/2$, where $u_{i,j}$ indicates the partial differentiation of u_i with respect to position x_j. The components of electric field are given by $E_i=- \varphi_{,i}$ where φ is the electric potential. The elasticity matrix at constant electric field is $[\mathbf{c}^E]$, the dielectric permittivity matrix at constant strain is $[\boldsymbol{\varepsilon}^S]$ and **[e]** is the matrix of piezoelectric coefficients.

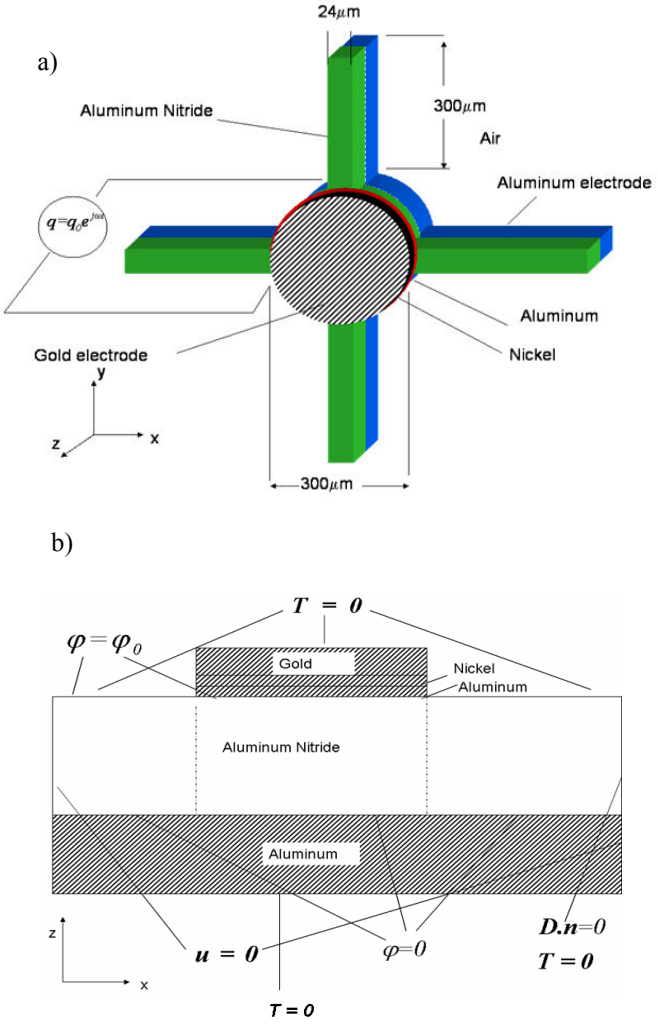

Figure 2. a) Schematic of the AlN trampoline resonator with gold-aluminum electrodes used in the 3D FEM simulations. b) Mechanical and electrical boundary enforced in the simulations.

As it is well known, (1) cannot be solved in closed form for the mechanical displacements and the electrical potential for any but the simplest geometries and boundary conditions [10] unlike the one-dimensional case which can be solved exactly. We now specify the one dimensional equations relevant to a structure which includes electrodes. We point out that comparing a damped three-dimensional simulation model to an undamped one-dimensional analytical model creates no problem. This is because it can be shown that for a lightly damped system as the one at hand, the damped and undamped resonant frequencies only differ slightly [23].

ONE-DIMENSIONAL SOLUTION OF COMPOSITE STRUCTURE

Figure 3 is a schematic of the FBAR structure we analyze. It consists of a piezoelectric layer of thickness h_2 with a top electrode and a bottom electrode respectively h_1 and (h_4-h_2) μm thick and placed in an electrical field directed along the x_3 (-z) axis. We utilize the subscript 'p' for the quantities pertaining to the piezoelectric layer and the subscript 'i' or 'e' for the top or bottom electrode respectively. The electrode's faces are oriented orthogonally to the axis of polarization. The one-dimensional model is valid for our structure because the thickness of the piezoelectric layer where acoustic waves are produced is much less that all other characteristic lengths and the electrodes' lengths are much greater than their thickness [10]. Additionally, the electrical field is only directed along the polarization axis which is a necessary assumption for the one-dimensional model to hold.

Equations governing the piezoelectric layer

Assuming that in the piezoelectric layer, the displacement u_p and the electric field E_p have a harmonic distribution of frequency ω, the relevant one-dimensional equations for the stress T_p and the electrical displacement D_p are

$$\begin{aligned} T_p(x_3,t)&=T_{33}=(C_{33}^E u_{3,3} - e_{33}E_3)e^{j\omega t} \\ D_p(x_3,t)&=D_3=(e_{33}u_{3,3}+\varepsilon_{33}^S E_3)e^{j\omega t} \end{aligned} \tag{2}$$

$$u_p(x_3,t)=u_3(x_3,t), \quad E_p(x_3,t)=E_3(x_3,t)= -\frac{\partial \varphi_p}{\partial x_3}$$

where $u_p(x_3,t)=u_3(x_3,t), \quad E_p(x_3,t)=E_3(x_3,t)= -\dfrac{\partial \varphi_p}{\partial x_3}$

and t represents time.
For simplicity, the superscripts *E* and *S* are omitted onward.

In the absence of body forces, Newton's law is

$$T_{33,3} = \rho_p u_{3,tt} \tag{3}$$

where ρ_p is the piezoelectric material's density and in the absence of free charge in the material Gausses' law is

. (4)

Substitution of (2) in (3) and (4) yields the following system of equations

$$\begin{aligned} C_{33}u_{3,33}+e_{33}\varphi_{p,33}&=-\rho_p\omega^2 u_3 \\ e_{33}u_{3,33}-\varepsilon_{33}\varphi_{p,33}&=0. \end{aligned} \tag{5}$$

Solutions for the displacement and the electric potential in the piezoelectric material may be written

$$u_p(x_3,t)=a_p e^{j(k_p x_3+\omega t)}+b_p e^{-j(k_p x_3-\omega t)}$$
$$\varphi_p(x_3,t)=\frac{e_p}{\varepsilon_p}u_p+ax_3+b, \quad (6)$$

where a_p, b_p, a and b are constants, $j=\sqrt{-1}$, $k_p=\omega/V_p$ is the wave number in the piezoelectric material, $V_p=\sqrt{(C_p^D/\rho_p}$ is the wave velocity and $C_p^D=C_p^E+e_p^2/\varepsilon_p$ is the material equivalent stiffness. Without any loss of generality, the constant b may be taken as zero.

Using (6), (2) can be rewritten as

$$T_p(x_3,t)=\left[j\omega Z_p\left(a_p e^{jk_p x_3}-b_p e^{-jk_p x_3}\right)+e_p a\right]e^{j\omega t}$$
$$D_p(x_3,t)=-\left(\varepsilon_p^S a\right)e^{j\omega t}, \quad (7)$$

where the mechanical impedance $Z_p=\rho_p V_p$ of the piezoelectric material has been introduced.

It can be shown [10] that for a moderate piezoelectric material (i.e. a piezoelectric material with an electromechanical coupling coefficient $K<0.3$, $K^2<10\%$ as is the case for AlN), (7) are more useful if written as

$$T_p(x_3,t)=\left[j\omega Z_p\left(a_p e^{jk_p x_3}-b_p e^{-jk_p x_3}\right)+e_p\frac{\varphi_0}{h_2}\right]e^{j\omega t}$$
$$D_p(x_3,t)=-\left(\varepsilon_p^S\frac{\varphi_0}{h_2}\right)e^{j\omega t}. \quad (8)$$

where φ_o is taken as the total electrical potential across the electrodes.

Equations governing the electrodes

Because a metal is a dielectric material, the equations governing the behavior of the electrodes can be obtained by letting the piezoelectric constant e_{33} in (2) to be zero. The stress T_s and the electrical displacement D_s in the electrodes are

$$T_S(x_3,t)=\left(C_S u_{S,3}\right)e^{j\omega t}$$
$$D_S(x_3,t)=\left(\varepsilon_S E_S\right)e^{j\omega t}. \quad (9)$$

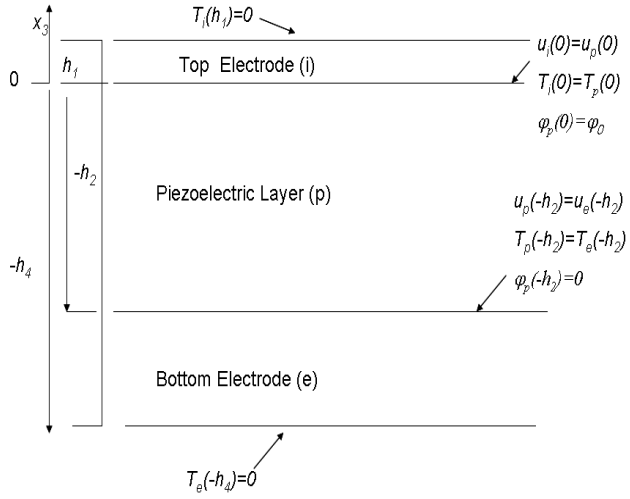

Figure 3. Schematic of the FBAR structure used in the one-dimensional analysis. The mechanical and electrical boundary conditions are shown.

The equations equivalent to (5) are

$$C_S u_{S,33}=-\rho_S\omega^2 u_S(x_3,t)$$
$$D_S(x_3,t)=0 \quad (10)$$

and those equivalent to (6) are

$$u_S(x_3,t)=a_S e^{j(k_s x_3+\omega t)}+b_s e^{-(k_s x_3-\omega t)}$$
$$T_S(x_3,t)=j\omega Z_S\left(a_s e^{jk_s x_3}-b_s e^{-jk_s x_3}\right)e^{j\omega t}. \quad (11)$$
$$(a_s, b_s \text{ constants}).$$

In (9)-(11), all the quantities hold analogous meanings as those previously described with the subscript *s* standing for either 'i' (the top electrode) or 'e' (the bottom electrode).

Solution for the three-layer composite structure

Complete solution of the problem at hand may be specified after the six unknown quantities a_p, b_p, a_i, b_i, a_e, b_e are known. They can be determined from six boundary conditions

$$\begin{cases} T_e(-h_4)=0 \\ u_p(-h_2)=u_e(-h_2) \\ T_p(-h_2)=T_e(-h_2) \\ u_p(0)=u_i(0) \\ T_p(0)=T_i(0) \\ T_i(h_1)=0. \end{cases} \quad (12)$$

The first and last conditions in (12) express that the external surfaces are stress free, while the second and third conditions represent the continuity of displacement and stress between the bottom electrode and the piezoelectric layer respectively

similarly to the fourth and fifth conditions which are the conditions pertaining to the piezoelectric material and the top electrode.

Defining the phase angle of each layer by

$$\phi_i = k_i h_1 \quad \phi_p = k_p h_2 \quad \phi_l = k_e h_4 \quad \phi_r = k_e h_2 , \quad (13)$$

and bringing out the electrodes respective elastic impedances $Z_s=\rho_e V_e$ and $Z_i=\rho_i V_i$, yields the following system of equations,

$$\begin{cases} a_e e^{-j\phi_l} - b_e e^{j\phi_l} = 0 \\ a_p e^{-j\phi_p} + b_p e^{j\phi_p} - a_e e^{-j\phi_r} - b_e e^{j\phi_r} = 0 \\ a_p e^{-j\phi_p} - b_p e^{j\phi_p} - (Z_e/Z_p)(a_e e^{-j\phi_r} - b_e e^{j\phi_r}) = \dfrac{e_p \varphi_0}{j\omega Z_p h_2} \\ a_p + b_p - a_i - b_i = 0 \\ a_p - b_p - (Z_i/Z_p)(a_i - b_i) = \dfrac{e_p \varphi_0}{j\omega Z_p h_2} \\ a_i e^{j\phi_i} - b_i e^{-j\phi_i} = 0. \end{cases} \quad (14)$$

Equation (14) is 6x6 system of algebraic equations which is assured a non trivial-solution provided its principal determinant vanish, namely if the following condition is enforced

$$\tan(\phi_l - \phi_r) = -\frac{(Z_i/Z_e)\tan\phi_i + (Z_p/Z_e)\tan\phi_p}{1-(Z_i/Z_p)\tan\phi_i \tan\phi_p}, \quad (15)$$

where $\phi_l - \phi_r = k_e(h_4 - h_2)$.

We note that the limit case where (h_4-h_2) tends to zero in (15) yields the relation

$$\tan\phi_i = -(Z_p/Z_i)\tan\phi_p , \quad (16)$$

a result that has be derived directly from the one-dimensional analysis of a two layer-structure [10] and corresponding to the case of a piezoelectric layer with one electrode.

Validation

To assess the validity of this rule (15) and to provide a mean of comparison between the predicted and the simulated data, we use aluminum nitride as the piezoelectric layer, gold for the top electrode and aluminum for the bottom electrode. The aluminum nitride layer (h_2) is 1.7 μm thick, the gold electrode thickness (h_1) varies from 0.0675 μm to 0.54 μm and the desired output is the aluminum electrode thickness (h_4-h_2). The results are shown in Figure 4. In the ratio H/h_2, H is the total thickness of the two electrodes $(h_1+(h_4-h_2))$.

We see that if the total thickness of the two electrodes is less than about 10% of that of the piezoelectric layer, there is no distinct advantage in using the new rule. Both the elementary and the new rule yield the same frequency decrease due to electrodes added mass. They also agree very well with the simulated data. When electrodes have thicknesses between 10 and 20% that of the piezoelectric layer, there is a slight improvement of prediction of mass loading effect using the new one-dimensional model: the new rule yields a higher value of f. To illustrate, if the piezoelectric layer is 1.7 μm and the two electrodes combined thickness is 0.3 μm (~18%), the elementary rule predicts a resonant frequency of 2. 26 GHz (0.71*3.185 GHz), while the new rule predicts that the device will resonate at 2.29 GHz (0.72*3.185 GHz). The trend continues even for electrodes thicknesses greater than 20% of the piezoelectric layer thickness and the deviation remains about constant after 25%. The results also agree perfectly with those obtained from the simulations. We note that electrodes which account for more than 25 % of the piezoelectric thickness are unpractical and that the results are only plotted to illustrate the trend. Too thick electrodes would result in a wave being generated and bouncing back between the electrodes boundaries producing a mechanism for high energy loss and defeating device performance enhancement.

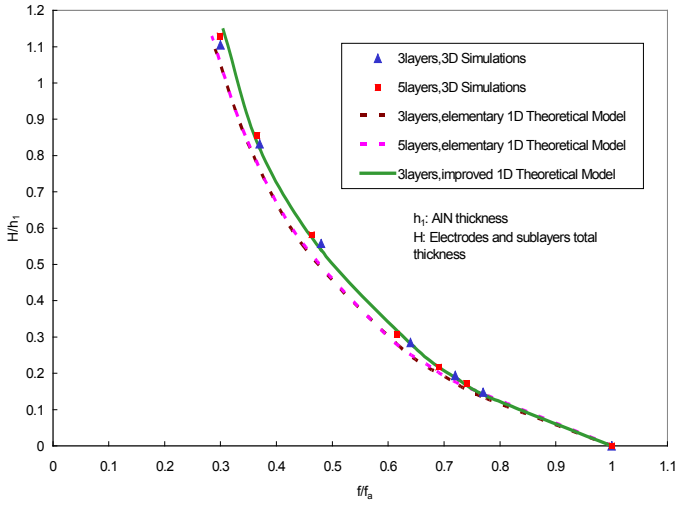

Figure 4. Comparison of one-dimensional analytical results with three-dimensional FEM simulations of AlN FBAR resonators in longitudinal resonance.

ACKNOWLEDGMENTS

This work was supported in part by the Defense Advanced Research Project Agency ONR/MINT under contract N66001-01-1 8965.

REFERENCES

[1] Nguyen, C. T.–C., 1998, "Microelectromechanical devices for wireless communications," *Proceedings IEEE International Microelectromech. Syst. Workshop*, Heidelberg, Germany, Jan. 25-29, pp. 1-7.

[2] Bannon, F.D., III, Clark, J.R., Nguyen, C. T.-C, Apr. 2000, "High-Q high frequency micromechanical filters", *IEEE J. Solid-State Circuits*, **vol. 35**, pp. 512-526.

[3] Wang, K., Wong, A-C., Nguyen, C. T.-C. , Sept. 2000, "VHF free-free beam high-Q micromechanical

resonators", *J. Microelectromech. Syst.*, **vol. 9**, pp. 347-360.

[4] Ruby, R. C. , Bradley, P. , Oshmyansky, Y. , Chien A., and Larson, J.D. III, 2001, "Thin film bulk wave acoustic resonators (FBAR) for wireless applications", *IEEE Ultrasonics Symposium*, Piscataway, NJ, pp. 813-821.

[5] Lakin, M., 2001, "Thin film resonators and high frequency filters, TFR Technologies, Inc.

[6] Antkowiak, B., Gorman, J.P., Varghese, Carter, D.J.D., Duwel, A.E., June 8-12, 2003, "Design of high-Q low-impedance, GHZ-range piezoelectric MEMS resonator", *12th Int. Conf. Solid State Sensors, Actuators and Microsystems*, Boston.

[7] Fattinger, G. G., Kaitila, J., Aigner, R. , Nesler, W. , 2003, "Thin film bulk acoustic wave devices for applications at 5.2 GHz", *IEEE Ultrasonics Symposium*, pp. 174 -177.

[8] Kim, H.H., Ju, B.K., Lee, Y. H., Lee, S.H., Lee, J.K., Kim, S.W., 2004, "Fabrication of suspended thin film resonator for application of RF bandpass filter", *Microelectronics Reliability,* **vol. 44**, pp. 237-243.

[9] Clark, J.R., Hsu, W., Abdelmoneum, A., Nguyen, C. T.-C., Dec. 2005, "High-Q UHF micromechanical radial-contour mode disk resonators", *J. Microelectromech. Syst*, **vol. 14,** pp. 1298-1310.

[10] Dieulesaint, E., Royer, D., 1980, *Elastic Waves in Solids*, John Willey & Sons, Chapt.7.

[11] Rosenbaum, F., 1988, *Bulk Acoustic Wave Theory and Devices*, Arthech House, Boston, Chap.4-5-10.

[12] Auld, B.A., 1990, *Acoustic Fields and Waves in Solids*, Volume I, 2nd ed. Krieger, Malabar, FL, Chapt. 8.

[13] Lukas, M. Olding, T., and Sayer, M., Tasker, R., Sherrit,S., 1999, "Thickness mode material constants of a supported piezoelectric film," *Journal of Applied Physics*, **vol. 85**, pp. 2835-2843A.

[14] N. Cleland, A. N., M. Pophristic, M., and Ferguson, I., Sept. 2001, "Single-crystal aluminum nitride nanomechanical resonators," **vol. 79**, pp. 2070-2072.

[15] Osbond, P., Beck, C.M., Brierley, C.J. Cox, M.R., Marsh, S. P., Shorrocks, N.M., 1999, "The Influence of ZnO and electrode thickness on the performance of thin film bulk acoustic wave resonators," *IEEE Ultrasonics Symposium*, pp. 911-914.

[16] Callaghan, L. A., Lughi, V., MacDonald, N. C., Clarke, D. R., 2006, "Beam-supported AlN thin film bulk acoustic resonators", *IEEE Trans. Ultrason. Ferroelect. Freq. Contr.*, **53**, pp. 1101-1007.

[17] Callaghan, L.A., 2005, "Design, fabrication and characterization of beam-supported aluminum nitride thin film bulk acoustic resonators", Ph. D. Dissertation, Dept. Mech. Eng., University of California Santa Barbara, Santa Barbara, CA.

[18] Lughi, V., 2006, "Aluminum nitride thin films for MEMS resonators: growth and characterization", Ph. D. Dissertation, Materials Dept., University of California Santa Barbara, Santa Barbara, CA.

[19] Kaplan, A., 2005,"Arrays of high-performance UHF aluminum nitride trampoline resonators with gold-aluminum electrodes", *Ph. D. Dissertation*, Dept. Mech. Eng., University of California Santa Barbara, Santa Barbara, CA.

[20] Ruimi, A., Liang, Y., and McMeeking, R.M., April 14-16, 2008, "UHF aluminum nitride FBAR trampoline-shape resonators with gold-aluminum electrodes and silicon substrate with through thickness vibrations: computational performance", *Proceedings of the International Conference on Smart Materials and Adaptive Structures*, Tangiers, Morocco.

[21] Abaqus Explicit/User's Manual, Version 6.4, Hibbitt, Karlson & Sorensen, Inc. 2003.